HHS Public Access

Author manuscript

Neuroimage. Author manuscript; available in PMC 2018 September 01.

Published in final edited form as:

Neuroimage. 2017 September ; 158: 232–241. doi:10.1016/j.neuroimage.2017.06.060.

Magnetic Resonance Imaging of Odorant Activity-Dependent Migration of Neural Precursor Cells and Olfactory Bulb Growth

Nikorn Pothayee[a], **Diana Cummings**[b], **Timothy Schoenfeld**[c], **Stephen Dodd**[a], **Heather Cameron**[c], **Leonardo Belluscio**[b], and **Alan Koretsky**[a]

[a]Laboratory of Functional and Molecular Imaging, National Institute of Neurological Disorders and Stroke, National Institutes of Health, Bethesda, MD 20892

[b]Developmental Neural Plasticity Section, National Institute of Neurological Disorders and Stroke, National Institutes of Health, Bethesda, MD 20892

[c]Section on Neuroplasticity, National Institute of Mental Health, National Institutes of Health, Bethesda, MD 20892

Abstract

Neural progenitors or neuroblasts are produced by precursor cells in the subventricular zone (SVZ) and migrate along the rostral migratory stream (RMS) to the olfactory bulbs (OB) throughout life. In the OB, these adult born neurons either die or replace existing olfactory interneurons, playing a critical role in the stabilization of OB circuitry. Although several aspects of the addition of new neurons into the OB have been studied, it is unclear whether long-distance activity from the OB can regulate the influx of migrating neuroblasts along the RMS. In this study, iron oxide-assisted MRI was used to track the migration of neuroblasts in combination with reversible naris occlusion to manipulate odorant-induced activity. It was found that decreasing olfactory activity led to a decrease in the rate of neuroblast migration along the RMS. Removal of the naris occlusion led to an increase in migratory rate back to control levels, indicating that olfactory activity has regulatory function on neuroblast migration in the RMS. Blocking odorant activity also led to an arrest in OB growth and re-opening the block led to a rapid re-growth returning the bulb size to control levels. Furthermore, pharmacogenetic elimination of the neuroblasts demonstrated that they were required for re-growth of the bulb following sensory deprivation. Together, these results show that sensory activity, neural migration and OB growth are tightly coupled in an interdependent manner.

Keywords

cell tracking; neuroblasts; rostal migratory stream; olfactory bulb; neurogenesis

Corresponding author: Alan P. Koretsky, Laboratory of Functional and Molecular Imaging, National Institute of Neurological Disorders and Stroke, National Institutes of Health, Building 10, Room B1D728, 10 Center Drive, MSC 1065, Bethesda, MD 20892-106.

1. Introduction

The olfactory bulb (OB) is the first brain area required for processing odor information. Odorants bind to receptors on olfactory sensory neurons in the nasal epithelium and project their axons to the glomerular layer of the OB. Mitral cells relay sensory inputs from the glomerular layer to the piriform cortex in the brain. Throughout life, the OB displays remarkable plasticity including regeneration of olfactory neurons and integration of adult born neurons by ongoing neurogenesis in the subventricular zone (SVZ) lining the lateral ventricle wall of the forebrain (Lois and Alvarez-Buylla 1994). In the SVZ, neural stem cells give rise to neural precursor cells called neuroblasts, which organize themselves into chains as they migrate along the rostal migratory stream (RMS) (Lois and Alvarez-Buylla 1994, Lois, Garcia-Verdugo et al. 1996). These neuroblasts migrate tangentially into the OBs (Doetsch and Alvarez-Buylla 1996, Lois, Garcia-Verdugo et al. 1996, Peretto, Merighi et al. 1997) and then migrate radially to their specific destinations within the different layers of the OB, primarily the glomerular layer (GL) and granule cell layer (GCL)(Batista-Brito, Close et al. 2008). These new neurons integrate into microcircuits and participate in odor processing (Livneh, Adam et al. 2014). In addition, these new neurons are critical for proper formation and maintenance of the intrabulbar connectivity map (Cummings and Belluscio 2008, Cummings and Belluscio 2010).

Olfactory activity has been identified as a key regulator of survival of neural progenitors, their final cell type distribution, and their turnover in the olfactory bulb (Yamaguchi and Mori 2005). However, little is known about the effects of olfactory activity on the dynamics of cell migration along the SVZ-RMS-OB pathway. While dynamics of neuroblast migration have been elucidated in acute slice cultures (Luskin and Boone 1994, Koizumi, Higginbotham et al. 2006, Nam, Kim et al. 2007, Martinez-Molina, Kim et al. 2011, Khlghatyan and Saghatelyan 2012), assessing the effects of olfactory input on RMS dynamics *in vivo* has been challenging due to a lack of tools that can monitor the long migratory path and that allow for longitudinal experimentation in live animals. Two-photon imaging techniques are useful for studying of the superficial areas in the OB such as the glomerular layer (Sawada, Kaneko et al. 2011, Liang, Li et al. 2016). However, these tools cannot image long-distance migration of the cells from the SVZ to the olfactory bulb in vivo.

In this study, we utilized neuroblast labeling with micron-sized iron oxide particles (MPIOs), which has enabled *in vivo* MRI imaging of cell migration along the RMS into the OB (Shapiro, Gonzalez-Perez et al. 2006, Sumner, Shapiro et al. 2009, Granot, Scheinost et al. 2011), in combination with a reversible naris occlusion model (Cummings, Henning et al. 1997) to investigate the effects of odorant-induced activity on growth of the OB and migration dynamics of new neurons. Blockade of olfactory activity in three-week-old rats by naris occlusion led to a cessation in growth of the affected OB and a significant decrease in the migration rates of neuroblasts along the RMS. Removal of the naris occlusion to restore normal olfactory sensory stimulation led to an increase in growth of the OB and an increase in migration rate. Furthermore, the importance of ongoing neurogenesis for the recovery of olfactory bulb size after removal of the naris occlusion was tested in a transgenic rat model whose neuroblasts could be genetically ablated and showed that ongoing neurogenesis is indeed required for the re-growth of the olfactory bulb following the reinstatement of normal

levels of olfactory activity. These results demonstrate the usefulness of combining MRI cell tracking with MRI anatomical measurement to elucidate a tight coupling of olfactory activity, neuroblast migration and maturation of the rodent olfactory bulb.

2. Materials and Methods

2.1 Animal procedures

All animal procedures were done according to the guidelines of Institute of Laboratory Research Council and approved by the Animal Care and Use Committee (ACUC) of the National Institute of Neurological Disorders and Stroke at the National Institutes of Health.

2.2 Unilateral naris occlusion

To deprive animals of olfactory sensory input, 3-week-old, male, Sprague-Dawley rats were subjected to reversible unilateral naris occlusion (Cummings, Henning et al. 1997, Marks, Cheng et al. 2006). Polyethylene tubing of various diameters was used to construct nose plugs, which were adjusted to fit the nostrils of the animals. The nose plugs were replaced every 5–6 days to keep up with the increasing size of the nostrils as the animals grew. MRI images of the OB were performed weekly following the occlusion to obtain a dynamic measurement of the change of OB volume. All MRI experiments were performed on an 11.7 T animal MRI system (30 cm 11.7 T horizontal magnet, Magnex Scientific, Oxford, England, MRI Electronics, Bruker Biospin, Billerica, MA), equipped with a 12-cm integrated gradient shim system (Resonance Research Inc, Billerica, MA). A custom-built volume transmit coil and a custom built, 2.5-cm-diameter, receive-only surface-coil were used for MRI. 3D gradient echo sequences were used for all MRI acquisitions. The following parameters were used: Field of View (FOV) = 1.92 cm × 1.92 cm × 1.92 cm, matrix size 256 × 256 × 256 (75-μm nominal isotropic resolution), 12.5 kHz bandwidth, echo time (TE) = 8 ms, repetition time (TR) = 25 ms, and flip angle = 8°. OB volumes were obtained from manually drawn serial voxel of interest (VOI) that covered the entire OB using the Medical Image Processing, Analysis, and Visualization (MIPAV) program (http://mipav.cit.nih.gov) (Saar, Cheng et al. 2015).

2.3 In situ MRI cell labeling with micron-sized iron oxide particles (MPIOs)

For *in situ* cell labeling, in one group of the animals 20-μL of MPIOs (average diameter of 1.63 μm, Bangs Laboratories, used as received) suspension were injected after 3 weeks of occlusion (6-weeks of age) into the lateral ventricle near SVZ (coordinate: AP+1.9 to +2.0, ML +1.9 to +2.0, DV −4.0 from bregma) ipsilateral to the side of the occluded naris. In the other two groups of animals, the naris plug was removed after 3 weeks of occlusion, to restore olfactory activity. MPIOs were injected 2 or 7 days prior to removal of the naris plug. MPIO injection allows a portion of the migrating neuroblasts to be labeled near the SVZ and then carry the MPIOs as they migrate into the OB. Serial *in vivo* MRI was performed to monitor the appearance of hypointense signal that was generated from MPIOs using the following parameter: Field of View (FOV) = 1.92 cm ×1.92 cm ×1.92 cm, matrix size 256 × 256 × 256 (75-μm isotropic resolution), 12.5 kHz bandwidth, echo time (TE) = 8 ms, repetition time (TR) = 25 ms, and flip angle = 8°. For detection of the migrating stream of neuroblasts, MRI was performed at 4–6 hours post-injection and then at 20–24 hours post-

injection. The rate of cell migration was calculated as the distance the migrating neurons traveled in the time between the two imaging sessions. The number of hypointense voxels within the OB was counted based on voxels that had 30% or more decrease in signal intensity. Three 75-μm thick MRI slices were combined through minimum intensity projections to increase counting efficiency minimizing the chance that repetitive counting of the same voxels occurred. It was assumed that each voxel with decreased signal intensity contained a single cell. The density of MPIO-containing cells was derived by dividing the number of spots by the OB volume.

2.4 Pharmacogenetic ablation of neurogenesis in GFAP-TK Transgenic rats and valganciclovir (VGCV) administration

Transgenic rats that express herpes simplex virus thymidine kinase under the glial fibrillary acidic protein (GFAP) promoter (GFAP-TK), on a Long-Evans background were used to elucidate the effect of neurogenesis on OB volume. VGCV treatment of GFAP-TK rats inhibits adult neurogenesis by selectively killing GFAP-expressing proliferating cells in the SV zone, as described previously (Snyder, Grigereit et al. 2016). Unilateral naris occlusion was introduced on the same day of the VGCV treatment on both transgenic (TK) and wild-type rats (WT). After 3 weeks of occlusion and VGCV treatment, the animals were sacrificed and perfused with 4% parafomaldehyle (PFA) in PBS containing 5 mM of gadolium-DTPA (Magnevist). To keep the OB tissue intact and prevent distortion of the OB, the brains were left in the skulls and transferred to a 50-mL conical tube. The same tube was then filled with the fixative containing gadolinium-DTPA. *Ex vivo* MRI was performed to obtain images of the OB using the following parameters: For *ex vivo* imaging the following MRI parameters were used: FOV = 2.56 cm^3, matrix size 3123, 20 kHz bandwidth, TE = 10 ms, TR = 25 ms, and flip angle = 30°. One set of control animals continued the VGCV treatment but had the naris plug removed for 3 weeks before perfusion. A second set of control animals had received 3 weeks of naris occlusion but no treatment with VGVC.

2.5 Immunohistochemistry

After the MRI acquisitions, animals were perfused transcardially with 1× PBS followed by 4% PFA. The brains were post-fixed, cryoprotected, sectioned (40 μm) coronally, and processed for immunofluorescence for neuroblast and interneurons. For immunostaining of neuroblasts, anti-doublecortin (DCX) (guinea pig anti-doublecortin, Millipore, antibodiy dilution 1:400) was used. For mature interneurons in the OB, anti-calretinin (rabbit anti-calretinin; Abcam; antibody dilution 1:2500) and anti-5T4 (mouse anti-5T4: Abcam; antibody dilution 1:1000) were used. Appropriate secondary antibodies conjugated to Cy3 (Jackson ImmunoResearch) were used for counter staining. Sections were mounted serially onto slides and coverslipped using Vectashield mounting medium (Vector Laboratories). Confocal images were collected with a Zeiss LSM 510 laser scanning confocal microscope using a 40×, 0.9 NA oil objective. Fluorescence images of doublecortin in the SVZ-RMS of GFAP-TK and WT rats were images on Nikon ECLIPES Ti microscope (Nikon, CA) using a 20× objective.

2.6 Statistical Analysis

The data obtained from the experiments are presented as the mean ± SD. Comparison among the groups was analyzed by Student's t-test and one-way ANOVA. Significance level was set at $p < 0.05$.

3. Results

3.1 MRI revealed dynamic changes in OB size following reversible activity deprivation

Previously it has been reported that naris occlusion leads to a smaller OB on the occluded side compared to the open, normal side (Frazier-Cierpial and Brunjes 1989, Cummings, Henning et al. 1997). This is due, at least in part, to a loss of interneuron and OB cells that results from a lack of sensory input (Frazier-Cierpial and Brunjes 1989, Fiske and Brunjes 2001). Although the smaller size of the affected OB has been reported previously following sensory deprivation, those results relied on histological evaluation and cross-animal comparison. Here, MRI was used to longitudinally monitor the changes in OB size throughout the course of sensory input manipulation starting in three-week-old rats (Fig. 1 A–D). One week after occlusion MRI results indicated that the size of OB ipsilateral to the occluded naris were smaller than the OB ipsilateral to the opened side. The difference in volumes became more pronounced after three weeks of occlusion. MRI measurement after removal of nose plugs after three weeks of olfactory deprivation indicated recovery of the OB volume.

The OB volume measured by MRI indicated that the OB size continued to increase during the occlusion on both sides (Fig. 1 E–F), but that the blocked side grew at a slower rate relative to the opened side. During the early time point of the occlusion, the growth rate of the OB ipsilateral to the occluded side was about 50% compared to the growth of the OB on the opened side. After three weeks of naris occlusion, the size of the blocked OB decreased to 20–30% of the size of the opened side. Consistent with a previous study (Cummings, Henning et al. 1997), the OB regained its size after normal levels of olfactory activity were restored. The recovery of OB volume was rapid with an increased growth rate occurring 1–2 weeks after naris plug removal (Fig. 1 G). By two weeks, the growth of the OB returned to the normal rate similar to the opened side and the volume returned to near control level. These results demonstrated that sensory deprivation caused by naris block led to a decrease in growth rate and the return of sensory activity by removal of the naris block resulted in an accelerated growth toward control sizes.

3.2 MPIO assisted MRI revealed odorant activity-dependent migration rates of neuroblasts along the RMS

In situ MRI cell labeling with MPIOs was used to monitor neuroblast migration *in vivo* as previously described (Shapiro, Gonzalez-Perez et al. 2006, Sumners, Shapiro et al. 2009) MPIOs were injected into the ventricles near the SVZ, which is sufficient to cause uptake into precursor cells in the SVZ enabling MRI at various time points after the injection to measure neuroblast dynamics. The rate measurement by MRI relied on measuring the distance that the leading edge of the dense cells moved by MRI over varying time intervals. Previously, it has been shown that movement of MRI contrast along the RMS requires cell

migration (Sumners, Shapiro et al. 2009). A portion of particles were taken up by cells enabling the detection of these cells by MRI as a hypointense signal due to a $T2^*$-shortening effect generated by the large magnetic field gradients from the MPIOs (Lauterbur, Bernado Jr. et al. 1986). To determine the time-course of neuroblast migration, serial MRI was performed at 4, 18, and 120 hours following the MPIO injection (Fig. 2). At 4 hours post-injection, the beginning of migration of labeled cells could just be detected as a hypointense stream of MPIO labeled cells leaving the SVZ (Fig. 2. B). At 18 hours post-injection, the stream of MPIO could be readily detected well into the RMS (Fig. 2 C) and after 120 hours, the MPIO labeled cells could be detected spreading throughout the OB (Fig. 2 D). From these measurements, it was revealed that neuroblasts migrate rapidly along the RMS and that MRI measure within one day following MPIO injection should be sufficient to determine migration rate within the RMS. The measurement of distance of the progression was used to provide an estimate of the rate of migration of MPIO labeled cells.

The migration rate along the RMS in animals that had undergone naris occlusion was compared to those that were occluded and reopened. After three weeks of occlusion, the animals were injected with MPIOs into the lateral ventricle on the same side as the occluded naris. Two groups of animals underwent a reopening of the naris block allowing restoration of olfactory activity with MPIO injections occurring two and seven days after removal of the naris plug. The effects of naris occlusion and reopening on cell migratory rate along the RMS are shown in Fig. 3A. A projection of five parasagittal MRI slices (75-μm thick) onto one plane using a minimum intensity projection available in MIPAV is shown in Fig. 3C–J. The projection was done to ensure that the entire RMS path was captured due to the curvature of the whole RMS stream. These serial MRI projections allowed for the measurements of the average cell migration rates across the groups of the animals (Fig. 3B). From these data, the average cell migration rate in the control animals was 120±5 μm/h. The average speed of migration dropped significantly to 89±4 μm/h in the animals that had unilateral naris blockade. The average migration speed in the animals with naris plugs removed after two days and seven days increased to 101±8 μm/h and 125±13 μm/h, respectively. Thus, the slowing in growth of the bulb was associated with a slowing of cell migration along the RMS. Conversely, return of olfactory activity caused a return of the migration rate to control levels as the bulb resumed its normal growth.

3.3 Migration of new cells radially into the OB was affected by naris block and return of olfactory activity

On reaching the OB, neuroblasts migrate radially into the OB as they exit from the subependymal layer, and continue to migrate into different layers of the OB (Lois and Alvarez-Buylla 1994). Fig. 4B and 4C show OB from the same animals that received MPIO injection and were imaged at one and two weeks post-injection. Clear hypointense voxels were detected throughout the bulb by two weeks post-injection. The RMS and subependymal region was defined from a medial plane of the OB (circled in white in Fig. 4). One week after leaving the SVZ and migrating into the OB, the neuroblasts are still primarily in the RMS. Between one week and two weeks after MPIO injection, cells begin to migrate to the outer layers of the OB. Histological evaluation of the OBs at 1 week (Fig.4 D, E, F) and 2 weeks (Fig. 4. G, H, I) post-injection showed that distributions of MPIO were

in good agreement with MRI and showed that the MPIOs in the OB are closely associated with DCX-expressing immature neurons. Further confocal analysis confirmed that MPIOs remained intracellular in appropriate cell types once they reached the OB (Fig. 5).

It is now well-established that iron oxide labeling of cells enables detection of individual cells (Dodd, Williams et al. 1999, Shapiro, Srktic et al. 2004). Many groups have reported detection of single cells in MPIO-labeled cells including hepatocytes transplanted into liver (Shapiro, Sharer et al. 2006), individual macrophages infiltrating the rejecting transplanted heart (Wu, Ye et al. 2006, Ye, Wu et al. 2008), single metastatic tumor cells in the brain and liver (Heyn, Ronald et al. 2006, Townson, Ramadan et al. 2009), as well as *in vivo* fates of various types of stem cells (Boulland, Leung et al. 2012, Tarulli, Chaudhuri et al. 2013, Chen, Lu et al. 2016). In all these cases the detection limit of MPIO-containing cells critically depends on the MRI resolution. In this work, 75-μm isotropic resolution was used to achieve enough resolution, which was important to quantify the hypointense voxels. The MPIO-labeled cells were spreading throughout in the OB and it was assumed that each hypointense voxel contained a single cell. An image voxel was considered to have a cell when there was a drop in signal intensity equal or greater than 30% below average background intensity in the local area being assessed (Fig. 6 A–E). These hypointense voxels were counted at various time points after MPIO injection. The count of MPIO labeled cells for the different times and groups were performed at various time-points (Fig. 6 G and F). During the first week, there were only a few MPIO labeled cells (5 to 9 hypointense pixels) detected in the OB of the animals across the groups. After two weeks, a number of MPIO labeled cells were detected; 31±9, 42±6, and 68±5 for the narisoccluded, control, and reopened groups, respectively. These MPIO-labeled signals continued to increase, and by six weeks post-labeling the numbers were 57±8, 68 ±5, and 127±5 spots for the narisoccluded, control, and reopened groups, respectively. There were less labeled cells in the animals that still had naris plugs in place when compared with the control animal (Fig. 6 F). However, when the volume of the OB was taken into the account, the densities of the labeled cells were the same between the narisoccluded and the control groups (Fig. 6 G). These results indicate that olfactory deprivation decreased the total number of cells entering the bulb but did not alter the density of new cells migrating into the OB. Removing the naris block led to an increase in the number of labeled neuroblasts that entered the OB. The numbers of labeled cells in these rats were almost double the numbers from the control group (Fig. 6 G). The rate of new cell addition within the reopened group was higher than the control and narisoccluded animals. By four weeks the rate of cell addition into the OB returned to the baseline. Therefore, a large increase in the number of new neurons entering the OB was associated with the increase in rate of growth of the OB after removal of the naris block.

3.4 The generation of new neurons that migrate into the OB is required to restore OB growth recovery following activity deprivation

The correlation of the recovery of OB volume with the increased addition of new neurons to the OB led to the hypothesis that the generation of new neurons is critical for restoration of OB growth after recovery from odorant-induced activity. To test this hypothesis, naris occlusion was performed in transgenic animals expressing herpes simplex virus thymidine kinase in GFAP-expressing cells enabling the production of new neuroblasts to be

pharmacogenetically abolished. Previous studies have shown that administration of VGCV in GFAP-TK mice leads to the complete ablation of new neuron production within the dentate gyrus and SVZ (Snyder, Soumier et al. 2011, Cummings, Snyder et al. 2014). Recently, a GFAP-TK transgenic rat model for specific inhibition of neurogenesis in the hippocampus has been described (Snyder, Grigereit et al. 2016). GFAP-TK rats were used to investigate the effects of neurogenesis on recovery of OB growth. GFAP-TK rats and wild-type (WT) littermates experienced naris closure from three to six weeks of age, followed by three weeks of recovery. All animals were given VGCV orally three times per week. After three weeks of VGCV treatment, immunostaining showed few doublecortin-expressing immature neurons remained in the SVZ and RMS indicating the effective elimination of neuroblast production within these two proliferative zones (Fig. 7 B–E).

After three weeks of VGVC administration, half of the animals in each group were sacrificed, and the OBs were imaged ex-vivo to get more accurate measures of the OB volume. Both WT and GFAP-TK rats that underwent three weeks of naris occlusion, and VGCV treatment had smaller OB sizes, relative to the OB on the sides that were not occluded. Following removal of nose plugs, the OB volume in WT rats regrew (from 34±1.7 to 39±0.9 mm^3, $p < 0.005$) similar to what was seen in experiments described in Fig. 1. However, in GFAP-TK rats, whose neurogenesis was suppressed by the treatment with VGCV, there was no recovery in OB growth (genotype × treatment interaction, p=0.0006) after removal of the naris occlusion (Fig. 7 F–J). The results showed that without SVZ neurogenesis and a migration of new neurons into the OB, there was no recovery of the OB growth even though the afferent olfactory activity was returned. On the other hand, in wild-type rats whose SVZ neurogenesis and migration of neuroblasts into the OB remained intact, the OB regrew when olfactory activity was restored. Thus, these results indicate that inhibiting the production of new neurons and their migration into the OB led to elimination of the OB's ability to regrow following the return of olfactory input.

4. Discussion

In this study, changes in OB volume and neuroblast migration in response to naris occlusion were measured with MRI. The results showed coupling between olfactory input and migration rate of new neurons migrating into the OB, pointing to a potential new mechanism for the regulation of OB circuits. This is the first demonstration that modulation of olfactory input affects dynamics of cell migration along the RMS. While previous work has shown that sensory deprivation leads to smaller OB volumes compared to non-deprived OBs, the results here indicate that OB sizes are controlled by the growth rates of the OB during occlusion and reopening.

It is well-established that naris occlusion lead to decrease in odorant-induce activity (Guthire, Wilson et al. 1990, Philpot, Foster et al. 1997, Cheetam, Park et al. 2016). This paradigm has been shown to lead a smaller OB on the blocked side, decreased olfactory neuron turnover, and destabilization of OB circuitry associated with decreased integration of adult born neurons (Cummings, Henning et al. 1997, Fiske and Brunjes 2001). Previous studies have also reported that granule cells require olfactory activity for their survival (Petreanu and Alvarez-Buylla 2002). Therefore, an explanation for a reduction in OB sizes

(relative to control OB) can be attributed to loss of granule cells and their integration into the granule cell layer (GCL). Remarkably, the block of activity lead a large inhibition in the normal growth (at least in these young adult rodents). Although there was a decrease in new cell integration into the OB, overall density of new neurons did not change indicating an active coupling of the OB growth to the number of new neurons.

It has been shown that long-distance activity from the OB is not required for migration along RMS (Kirschenbaum, Doetsch et al. 1999, Petreanu and Alvarez-Buylla 2002). However, modulatory effects on the RMS migration dynamics have not previously been studied. To investigate the relationship between odorant-induced activity and migration dynamics of new neurons, we used iron oxide assisted MRI to the migration rate of neuroblasts along the RMS. In normal rat, the top speed of approximately 120 μm/h was observed and consistent with the values obtained from *in vitro* measurement using slice culture, which have reported values ranging from 70–120 μm/h (Wichterle, Garcia-Verdugo et al. 1997, Nam, Kim et al. 2007). The results here were in good agreement with *in vivo* MRI measurement of neural precursor cell migration in mice, based on a similar approach of MRI cell labeling that reported a migration speed of 100 μm/h (Nieman, Shyu et al. 2010). By combining odorant activity manipulation with MRI, we observed that the rate of migration within the RMS was significantly affected by olfactory input level. Studies have shown that lack of olfactory activity can lead to an increase in cell death at all levels along the SVZ-RMS pathway (Mandairon, Jourdan et al. 2003). This in turn could contribute to slowing the apparent migration of new cells along the RMS. Alternatively, it is possible that there is a modulation of the migration pathway via chemoattractive and chemorepulsive factors that have been shown to influence migration in the RMS (Nguyen-Ba-Charvet, Picard-Riera et al. 2004) and whose release could be activity dependent. However, studies show that even after removal of the olfactory bulb, precursors continue to divide in the SVZ and migrate through the RMS (Kirschenbaum, Doetsch et al. 1999) suggesting that these diffusible factors are not essential but may modulate the migration. Alternative mechanisms by which olfactory activity could regulate the RMS flow is direct modulatory input from the anterior olfactory nucleus (AON). Since the RMS pathway goes through the AON, which receives significant projections from mitral/tuft cells in the OB (Schoenfeld and Macrides 1984, Shipley and Ennis 1996, Brunjes, Illig et al. 2005), it is possible that the AON could be induced to release modulatory factors to the RMS in response to changes in olfactory sensory level. Although it is unclear how olfactory activity affects the RMS migration rate, the results here suggest the olfactory activity has a quantitative effect on overall dynamics of cell migration along the RMS. Importantly, the change in migration rates of the neuroblasts is coupled to the change in growth rates of the bulb implying that migratory rate of new neurons could regulate OB growth.

MRI of MPIO labeled cells was also used to measure the degree of cell integration into the olfactory bulb once the neuroblasts depart the RMS. For this measurement, it was assumed that every hypo-intense voxel was due to a single labeled cell. Potential limitations for MRI-based cell counting are that labeling efficiency and detectability can change and have been shown to vary depending on labeling conditions (Vreys, Vande Velde et al. 2010). Another potential concern is specificity of labeling. For example, microglia and microphages, which commonly phagocytize the foreign objects in the brain, could internalize the MPIOs. The

third issue is that the criteria used to count cells relied on a 30% decrease in signal and it is likely that some cells were missed due to varying amounts of iron in the MPIOs. Lastly, there is a concern that signal could be diluted as cells divide and signals in the daughter cells reduces after every cell division. Advances in MRI reporter genes should prevent such signal dilution (Vande Velde, Rangarajan et al. 2011, Vandsburger, Radoul et al. 2013,) To make the detection of cells as robust as possible it is important to maximize MRI resolution as possible (Dodd, Williams et al. 1999, Shapiro, Skrtic et al. 2004), therefore sufficient imaging time was taken to acquire 75-μm isotropic resolution. Numerous reports indeed have shown that MPIO-labeled single cell signal can be detected when using appropriate resolution (Nieman, Shyu et al. 2010, Granot, Scheinost et al. 2011). New strategies to use more uniform particles with higher iron content should alleviate these issues in the future (Zabow, Dodd et al. 2011). Additionally, better image analysis schemes might also aid with quantification of cells (Afridi, Ross et al. 2016). Despite these caveats, the results obtained from MRI showed that an increase in the integration of new cells coincided with the regrowth of the OB. This is consistent with previous findings from other groups that utilized immunohistochemistry and thymidine-based labeling techniques (Cummings, Henning et al. 1997, Fiske and Brunjes 2001). Furthermore, MRI measurement also showed that integration of the new cells into the OB layers did not take place until about one week after the time of their exit from the SVZ, consistent with previous reports on the time course of neuroblast migration using histological methods (Luskin 1993, Lois, Garcia-Verdugo et al. 1996, Winner, Cooper-Kuhn et al. 2002). Importantly, our results showed a correlation between odorant-induced activity and integration of new cells into the OB. Activity likely regulates integration of new neurons by controlling their survival and synaptic connectivity (Petreanu and Alvarez-Buylla 2002, Yamaguchi and Mori 2005, Kelsch, Lin et al. 2009). It has been shown that brain-derived neurotrophic factor (BDNF) is down-regulated during sensory deprivation (McLean, Darby-King et al. 2001). Given the roles of BDNF in neuronal survival and synaptic development, its expression in response to olfactory sensory level may have a direct impact on integration of new neurons that radially migrate into the OB. It may be possible that activity regulate other neurotrophic factors such as glia-derived neurotrophic factor (GDNF), hepatocyte growth factor (HGF), insulin-like growth factor (IGF-1), which are important for neuroblast migration and neurogenesis in the OB (Paratcha, Ibáñez et al. 2006, Garzotto, Giacobini et al. 2008, Hurtado-Chong, Yusta-Boyo et al. 2009).

Tight coupling between OB growth and migration of new neurons suggests that the migration of new cells into the OB is required for OB re-growth following odorant deprivation. Indeed, we observed that production of new neurons and their migration into the OB were required for OB regrowth during the return of sensory activity. Although the degree to which increases in OB volume are caused by the integration of new neurons remains unclear. The primary target of SVZ neurogenesis is the addition of new neurons into GCL, though a small portion of new neurons were added into glomerular layer (GL). Thus, it is possible that the OB volume that re-grew may be attributed to the new addition of new neurons in GCL. Additional contribution of the anatomical recovery of the bulb volume could be re-innervation of olfactory sensory neurons through the olfactory nerve layer (ONL) (Cummings, Henning et al. 1997, Cummings and Belluscio 2010). However, the fact that we did not observe any recovery of OB volume when the production of new neuron was

ablated indicating that the addition of new neurons is critical for the recovery of glomeruli and axonal projection from OSN after renewal of odorant-induced activity. Using better strategies to delineate volume changes in a layer-specific manner could undoubtedly provide insight into this question. Manganese-enhance MRI (MEMRI) has been shown to provide excellent cytoarchitecture of the OB layers *in vivo* (Aoki, Wu et al. 2004, Chuang, Belluscio et al. 2010) and has been used to demonstrate laminar-specific effects during degeneration of the OB (Saar, Cheng et al. 2015). Thus, combining single-cell MRI tracking with MEMRI could provide insight into laminar specific migration of new neurons in response to odorant-induced activity.

5. Conclusion

Until recently, endogenous neural progenitors were routinely studied using histological sections or slice cultures. In this study, we demonstrate that the cell tracking can be combined with other anatomical and functional MRI tools to elucidate effects of olfactory activity level on cell migration dynamics and their influences on OB growth rate. The ability to complete longitudinal *in vivo* experiments using MRI should afford interesting new avenues for study. Our results demonstrate a tight regulation of olfactory activity on the migration of new cells and the gross anatomical size of the OB show the potential of this approach.

Acknowledgments

This work was supported by the Intramural Research Program of the National Institutes of Health, National Institute of Neurological Disorders and Stroke, and the National Institute of Mental Health. The authors express thanks to Nadia Bouraoud and Kathy Sharer for their technical assistance.

References

Afridi MJ, Ross A, Liu X, Bennewitz MF, Shuboni DD, Shapiro EM. Intelligent and automatic in vivo detection and quantification of transplanted cells in MRI. Magn Reson Med. 2016; doi: 10.1002/mrm.26571

Aoki I, Wu YJ, Silva AC, Lynch RM, Koretsky AP. In vivo detection of neuroarchitecture in the rodent brain using manganese-enhanced MRI. Neuroimage. 2004; 22(3):1046–1059. [PubMed: 15219577]

Batista-Brito R, Close J, Machold R, Fishell G. The distinct temporal origins of olfactory bulb interneuron subtypes. J Neurosci. 2008; 28(15):3966–3975. [PubMed: 18400896]

Boulland JL, Leung DS, Thuen M, Vik-Mo E, Joel M, Perreault MC, Langmoen IA, Haraldseth O, Glover JC. Evaluation of intracellular labeling with micron-sized particles of iron oxide (MPIOs) as a general tool for in vitro and in vivo tracking of human stem and progenitor cells. Cell Transplant. 2012; 21(8):1743–1759. [PubMed: 22490338]

Brunjes PC, Illig KR, Meyer EA. A field guide to the anterior olfactory nucleus (cortex). Brain Res Brain Res Rev. 2005; 50(2):305–335. [PubMed: 16229895]

Chen X, Lu M, Ma N, Yin G, Cui C, Zhao S. Dynamic Tracking of Injected Mesenchymal Stem Cells after Myocardial Infarction in Rats: A Serial 7T MRI Study. Stem Cells Int. 2016; 2016:4656539. [PubMed: 27656215]

Cheetham CE, Park U, Belluscio L. Rapid and continuous activity-dependent plasticity of olfactory sensory input. Nat Commun. 2016; 7:10729. [PubMed: 26898529]

Chuang KH, Belluscio L, Koretsky AP. In vivo detection of individual glomeruli in the rodent olfactory bulb using manganese enhanced MRI. Neuroimage. 2010; 49(2):1350–1356. [PubMed: 19800011]

Cummings DM, Henning HE, Brunjes PC. Olfactory bulb recovery after early sensory deprivation. J Neurosci. 1997; 17(19):7433–7440. [PubMed: 9295389]

Cummings DM, Belluscio L. Charting plasticity in the regenerating maps of the mammalian olfactory bulb. Neuroscientist. 2008; 14(3):251–263. [PubMed: 18420836]

Cummings DM, Belluscio L. Continuous neural plasticity in the olfactory intrabulbar circuitry. J Neurosci. 2010; 30(27):9172–9180. [PubMed: 20610751]

Cummings DM, Snyder JS, Brewer M, Cameron HA, Belluscio L. Adult Neurogenesis Is Necessary to Refine and Maintain Circuit Specificity. J Neurosci. 2014; 34(41):13801–13810. [PubMed: 25297106]

Dodd SJ, Williams M, Suhan JP, Williams DS, Koretsky AP, Ho C. Detection of single mammalian cells by high-resolution magnetic resonance imaging. Biophys J. 1999; 76(1 Pt 1):103–109. [PubMed: 9876127]

Doetsch F, Alvarez-Buylla A. Network of tangential pathways for neuronal migration in adult mammalian brain. Proc Natl Acad Sci U S A. 1996; 93(25):14895–14900. [PubMed: 8962152]

Fiske BK, Brunjes PC. Cell death in the developing and sensory-deprived rat olfactory bulb. J Comp Neurol. 2001; 431(3):311–319. [PubMed: 11170007]

Frazier-Cierpial L, Brunjes PC. Early postnatal cellular proliferation and survival in the olfactory bulb and rostral migratory stream of normal and unilaterally odor-deprived rats. J Comp Neurol. 1989; 289(3):481–492. [PubMed: 2808782]

Garzotto D, Giacobini P, Crepaldi T, Fasolo A, De Marchis S. Hepatocyte growth factor regulates migration of olfactory interneuron precursors in the rostral migratory stream through Met-Grb2 coupling. J Neurosci. 2008; 28(23):5901–5909. [PubMed: 18524894]

Granot D, Scheinost D, Markakis EA, Papademetris X, Shapiro EM. Serial monitoring of endogenous neuroblast migration by cellular MRI. Neuroimage. 2011; 57(3):817–824. [PubMed: 21571076]

Guthrie KM, Wilson DA, Leon M. Early unilateral deprivation modifies olfactory bulb function. J Neuro Sci. 1990; 10:3402–3412.

Heyn C, Ronald JA, Ramadan SS, Snir JA, Barry AM, MacKenzie LT, Mikulis D, Palmieri DJ, Bronder JL, Steeg PS, Yoneda T, MacDonald IC, Chambers AF, Rutt BK, Foster PJ. In vivo MRI of cancer cell fate at the single-cell level in a mouse model of breast cancer metastasis to the brain. Magn Reson Med. 2006; 56(5):1001–1010. [PubMed: 17029229]

Hurtado-Chong A, Yusta-Boyo MJ, Vergano-Vera E, Bulfone A, de Pablo F, Vicario-Abejon C. IGF-I promotes neuronal migration and positioning in the olfactory bulb and the exit of neuroblasts from the subventricular zone. Eur J Neurosci. 2009; 30(5):742–755. [PubMed: 19712103]

Kelsch W, Lin CW, Mosley CP, Lois C. A critical period for activity-dependent synaptic development during olfactory bulb adult neurogenesis. J Neurosci. 2009; 29(38):11852–11858. [PubMed: 19776271]

Khlghatyan J, Saghatelyan A. Time-lapse imaging of neuroblast migration in acute slices of the adult mouse forebrain. J Vis Exp. 2012; (67):e4061. [PubMed: 23007608]

Kirschenbaum B, Doetsch F, Lois C, Alvarez-Buylla A. Adult subventricular zone neuronal precursors continue to proliferate and migrate in the absence of the olfactory bulb. J Neurosci. 1999; 19(6): 2171–2180. [PubMed: 10066270]

Koizumi H, Higginbotham H, Poon T, Tanaka T, Brinkman BC, Gleeson JG. Doublecortin maintains bipolar shape and nuclear translocation during migration in the adult forebrain. Nat Neurosci. 2006; 9(6):779–786. [PubMed: 16699506]

Lauterbur PC, Bernado ML Jr, Mendoca Dias MH, Heldman AW. Microscopic NMR imaging of the magnetic fileds around magnetic particles. Proceedings of the 5th SMRM. 1986

Liang Y, Li K, Riecken K, Maslyukov A, Gomez-Nicola D, Kovalchuk Y, Fehse B, Garaschuk O. Long-term in vivo single-cell tracking reveals the switch of migration patterns in adult-born juxtaglomerular cells of the mouse olfactory bulb. Cell Res. 2016; 26(7):805–821. [PubMed: 27174051]

Livneh Y, Adam Y, Mizrahi A. Odor processing by adult-born neurons. Neuron. 2014; 81(5):1097–1110. [PubMed: 24508384]

Lois C, Alvarez-Buylla A. Long-distance neuronal migration in the adult mammalian brain. Science. 1994; 264(5162):1145–1148. [PubMed: 8178174]

Lois C, Garcia-Verdugo JM, Alvarez-Buylla A. Chain migration of neuronal precursors. Science. 1996; 271(5251):978–981. [PubMed: 8584933]

Luskin MB. Restricted proliferation and migration of postnatally generated neurons derived from the forebrain subventricular zone. Neuron. 1993; 11(1):173–189. [PubMed: 8338665]

Luskin MB, Boone MS. Rate and pattern of migration of lineally-related olfactory bulb interneurons generated postnatally in the subventricular zone of the rat. Chem Senses. 1994; 19(6):695–714. [PubMed: 7735848]

Mandairon N, Jourdan F, Didier A. Deprivation of sensory inputs to the olfactory bulb up-regulates cell death and proliferation in the subventricular zone of adult mice. Neuroscience. 2003; 119(2):507–516. [PubMed: 12770564]

Marks CA, Cheng K, Cummings DM, Belluscio L. Activity-dependent plasticity in the olfactory intrabulbar map. J Neurosci. 2006; 26(44):11257–11266. [PubMed: 17079653]

Martinez-Molina N, Kim Y, Hockberger P, Szele FG. Rostral migratory stream neuroblasts turn and change directions in stereotypic patterns. Cell Adh Migr. 2011; 5(1):83–95. [PubMed: 21045564]

McLean JH, Darby-King A, Bonnell WS. Neonatal olfactory sensory deprivation decreases BDNF in the olfactory bulb of the rat. Brain Res Dev Brain Res. 2001; 128(1):17–24. [PubMed: 11356258]

Nam SC, Kim Y, Dryanovski D, Walker A, Goings G, Woolfrey K, Kang SS, Chu C, Chenn A, Erdelyi F, Szabo G, Hockberger P, Szele FG. Dynamic features of postnatal subventricular zone cell motility: a two-photon time-lapse study. J Comp Neurol. 2007; 505(2):190–208. [PubMed: 17853439]

Nguyen-Ba-Charvet KT, Picard-Riera N, Tessier-Lavigne M, Baron-Van Evercooren A, Sotelo C, Chedotal A. Multiple roles for slits in the control of cell migration in the rostral migratory stream. J Neurosci. 2004; 24(6):1497–1506. [PubMed: 14960623]

Nieman BJ, Shyu JY, Rodriguez JJ, Garcia AD, Joyner AL, Turnbull DH. In vivo MRI of neural cell migration dynamics in the mouse brain. Neuroimage. 2010; 50(2):456–464. [PubMed: 20053381]

Paratcha G, Ibanez CF, Ledda F. GDNF is a chemoattractant factor for neuronal precursor cells in the rostral migratory stream. Molecular and Cellular Neuroscience. 2006; 31(3):505–514. [PubMed: 16380265]

Peretto P, Merighi A, Fasolo A, Bonfanti L. Glial tubes in the rostral migratory stream of the adult rat. Brain Res Bull. 1997; 42(1):9–21. [PubMed: 8978930]

Petreanu L, Alvarez-Buylla A. Maturation and death of adult-born olfactory bulb granule neurons: role of olfaction. J Neurosci. 2002; 22(14):6106–6113. [PubMed: 12122071]

Philpot BD, Foster TC, Brunjes PC. Mitral/tufted cell activity is attenuated and becomes uncoupled from respiration following naris closure. J Neurobiol. 1997; 33(4):374–386. [PubMed: 9322155]

Saar G, Cheng NL, Belluscio L, Koretsky AP. Laminar specific detection of APP induced neurodegeneration and recovery using MEMRI in an olfactory based Alzheimer's disease mouse model. Neuroimage. 2015; 118:183–192. [PubMed: 26021215]

Sawada M, Kaneko N, Inada H, Wake H, Kato Y, Yanagawa Y, Kobayashi K, Nemoto T, Nabekura J, Sawamoto K. Sensory input regulates spatial and subtype-specific patterns of neuronal turnover in the adult olfactory bulb. J Neurosci. 2011; 31(32):11587–11596. [PubMed: 21832189]

Schoenfeld TA, Macrides F. Topographic organization of connections between the main olfactory bulb and pars externa of the anterior olfactory nucleus in the hamster. J Comp Neurol. 1984; 227(1): 121–135. [PubMed: 6470206]

Shapiro EM, Skrtic S, Sharer K, Hill JM, Dunbar CE, Koretsky AP. MRI detection of single particles for cellular imaging. Proc Natl Acad Sci U S A. 2004; 101(30):10901–10906. [PubMed: 15256592]

Shapiro EM, Gonzalez-Perez O, Manuel Garcia-Verdugo J, Alvarez-Buylla A, Koretsky AP. Magnetic resonance imaging of the migration of neuronal precursors generated in the adult rodent brain. Neuroimage. 2006; 32(3):1150–1157. [PubMed: 16814567]

Shapiro EM, Sharer K, Skrtic S, Koretsly AP. In vivo detection of single cell by MRI. Magn Reson Med. 2006; 55(2):242–249. [PubMed: 16416426]

Shipley MT, Ennis M. Functional organization of olfactory system. J Neurobiol. 1996; 30(1):123–176. [PubMed: 8727988]

Snyder JS, Soumier A, Brewer M, Pickel J, Cameron HA. Adult hippocampal neurogenesis buffers stress responses and depressive behaviour. Nature. 2011; 476(7361):458–U112. [PubMed: 21814201]

Snyder JS, Grigereit L, Russo A, Seib DR, Brewer M, Pickel J, Cameron HA. A Transgenic Rat for Specifically Inhibiting Adult Neurogenesis. eNeuro. 2016; 3(3)

Sumner JP, Shapiro EM, Maric D, Conroy R, Koretsky AP. In vivo labeling of adult neural progenitors for MRI with micron sized particles of iron oxide: quantification of labeled cell phenotype. Neuroimage. 2009; 44(3):671–678. [PubMed: 18722534]

Tarulli E, Chaudhuri JD, Gretka V, Hoyles A, Morshead CM, Stanisz GJ. Effectiveness of micron-sized superparamagnetic iron oxide particles as markers for detection of migration of bone marrow-derived mesenchymal stromal cells in a stroke model. J Magn Reson Imaging. 2013; 37:1409–1418. [PubMed: 23712844]

Townson JL, Ramadan SS, Simedrea C, Rutt BK, MacDonald IC, Foster PJ, Chambers AF. Three-dimensional imaging and quantification of both solitary cells and metastases in whole mouse liver by magnetic resonance imaging. Cancer Res. 2009; 69(21):8326–8331. [PubMed: 19843857]

Vande Velde G, Rangarajan JR, Toelen J, Dresselaers T, Ibrahimi A, Krylychkina O, Vreys R, Van der Linden A, Maes F, Debyser Z, Himmelreich U, Baekelandt V. Evaluation of the specificity and sensitivity of ferritin as an MRI reporter gene in the mouse brain using lentiviral and adeno-associated viral vectors. Gene Therapy. 2011; 18:594–605. [PubMed: 21346786]

Vandsburger MH, Radoul M, Cohen B, Neeman M. MRI reporter genes: applications for imaging of cell survival, proliferation, migration and differentiation. NMR Biomed. 2013; 26(7):872–884. [PubMed: 23225197]

Vreys R, Vande Velde G, Krylychkina O, Vellema M, Verhoye M, Timmermans JP, Baekelandt V, Van der Linden A. MRI visualization of endogenous neural progenitor cell migration along the RMS in the adult mouse brain: validation of various MPIO labeling strategies. Neuroimage. 2010; 49(3): 2094–2103. [PubMed: 19850132]

Wichterle H, Garcia-Verdugo JM, Alvarez-Buylla A. Direct evidence for homotypic, glia-independent neuronal migration. Neuron. 1997; 18(5):779–791. [PubMed: 9182802]

Winner B, Cooper-Kuhn CM, Aigner R, Winkler J, Kuhn HG. Long-term survival and cell death of newly generated neurons in the adult rat olfactory bulb. Eur J Neurosci. 2002; 16(9):1681–1689. [PubMed: 12431220]

Wu YL, Ye Q, Foley LM, Hitchens TK, Sato K, Williams JB, Ho C. In situ labeling of immune cells with iron oxide particles: an approach to detect organ rejection by cellular MRI. Proc Natl Acad Sci U S A. 2006; 103(6):1852–1857. [PubMed: 16443687]

Yamaguchi M, Mori K. Critical period for sensory experience-dependent survival of newly generated granule cells in the adult mouse olfactory bulb. Proc Natl Acad Sci U S A. 2005; 102(27):9697–9702. [PubMed: 15976032]

Ye Q, Wu YL, Foley LM, Hitchens TK, Eytan DF, Shirwan H, Ho C. Longitudinal tracking of recipient macrophages in a rat chronic cardiac allograft rejection model with noninvasive magnetic resonance imaging using micrometer-sized paramagnetic iron oxide particles. Circulation. 2008; 118(2):149–156. [PubMed: 18591438]

Zabow G, Dodd SJ, Shapiro E, Moreland J, Koretsky AP. Microfabricated high-moment micrometer-sized MRI contrast agents. Magn Reson Med. 2011; 65(3):645–655. [PubMed: 20928829]

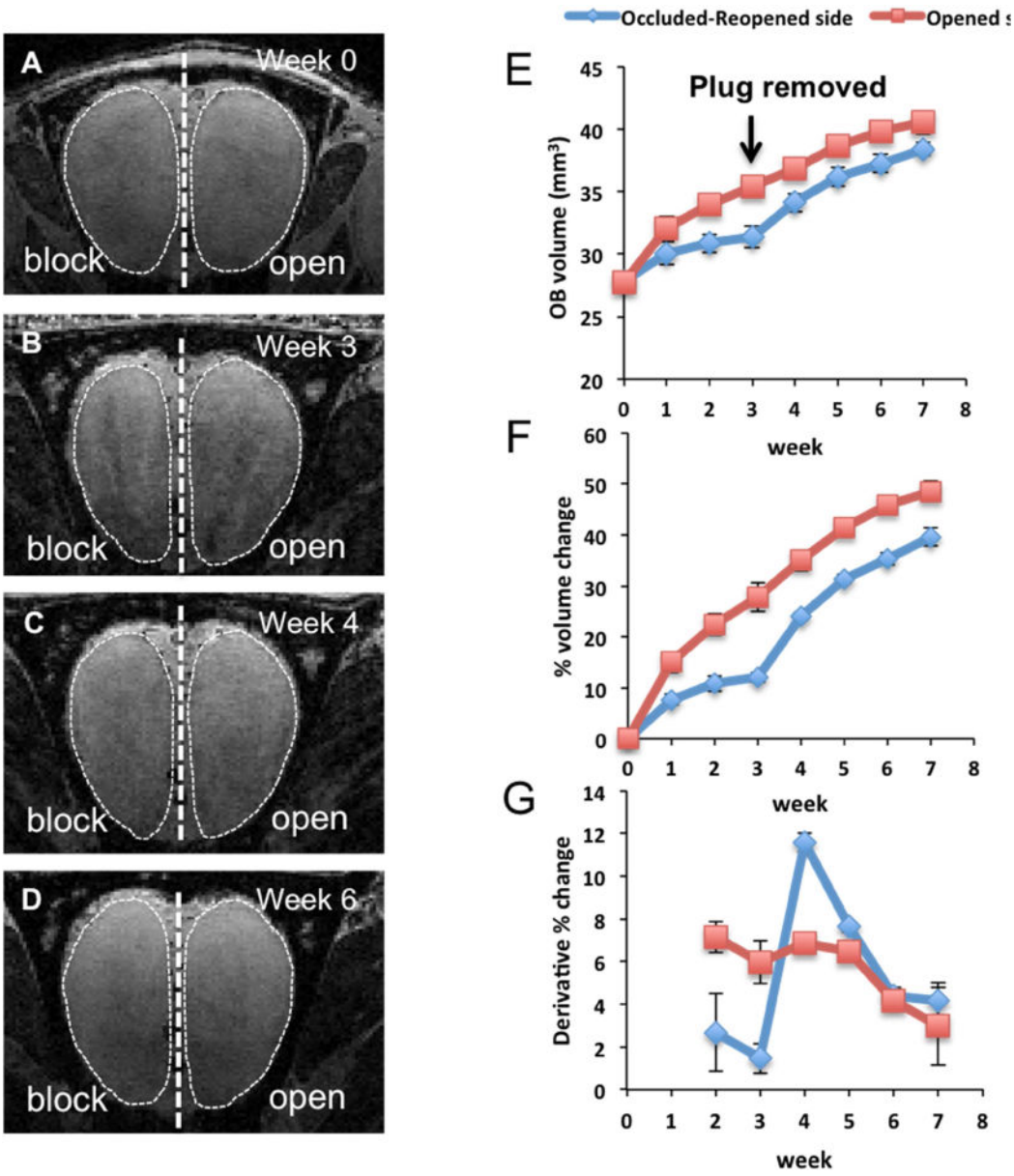

Figure 1.

Changes in OB volumes after unilateral naris occlusion in 3-week old rats. (A-B) MRI images of the OB during naris occlusion period (week 0 refers to initiation of naris occlusion). (C-D) images of the OB from the same animal during recovery period, during which the naris occlusion was reopened. E) Plot of average OB volume vs. time course of activity manipulation (N =6). F) Accumulative percentages of OB volume changes during the experiment. Percentage of changes in volume at each time point was normalized with the initial volume (at week 0). G) Derivatives of OB volume changes that occurred in each week was calculated by subtraction of the percentages of changes in volume (obtained from figure 1F) from previous week.

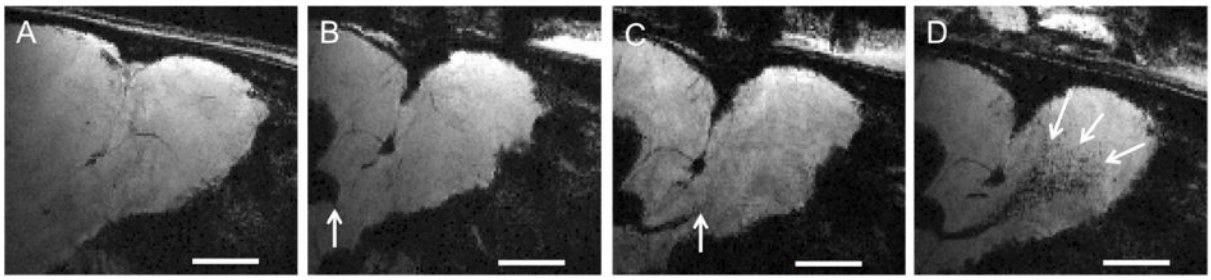

Figure 2.

Intraventricular injection of MPIOs near SVZ allow migrating neuroblasts to be labeled and detected with MRI in live rats. A) shows MRI image before injection of MPIO. Panel A represents MRI image of rat before MPIO injection. B-D) represent the same animal after injection of MPIOs into the lateral ventricle at different time points, with B = 4 hours, C = 18 hours, and D = 120 hours post-injection. MPIO(+) neuroblasts can be seen as a hypointense track migrating along the RMS into the OB (indicated by arrows). Scale bar = 2 mm.

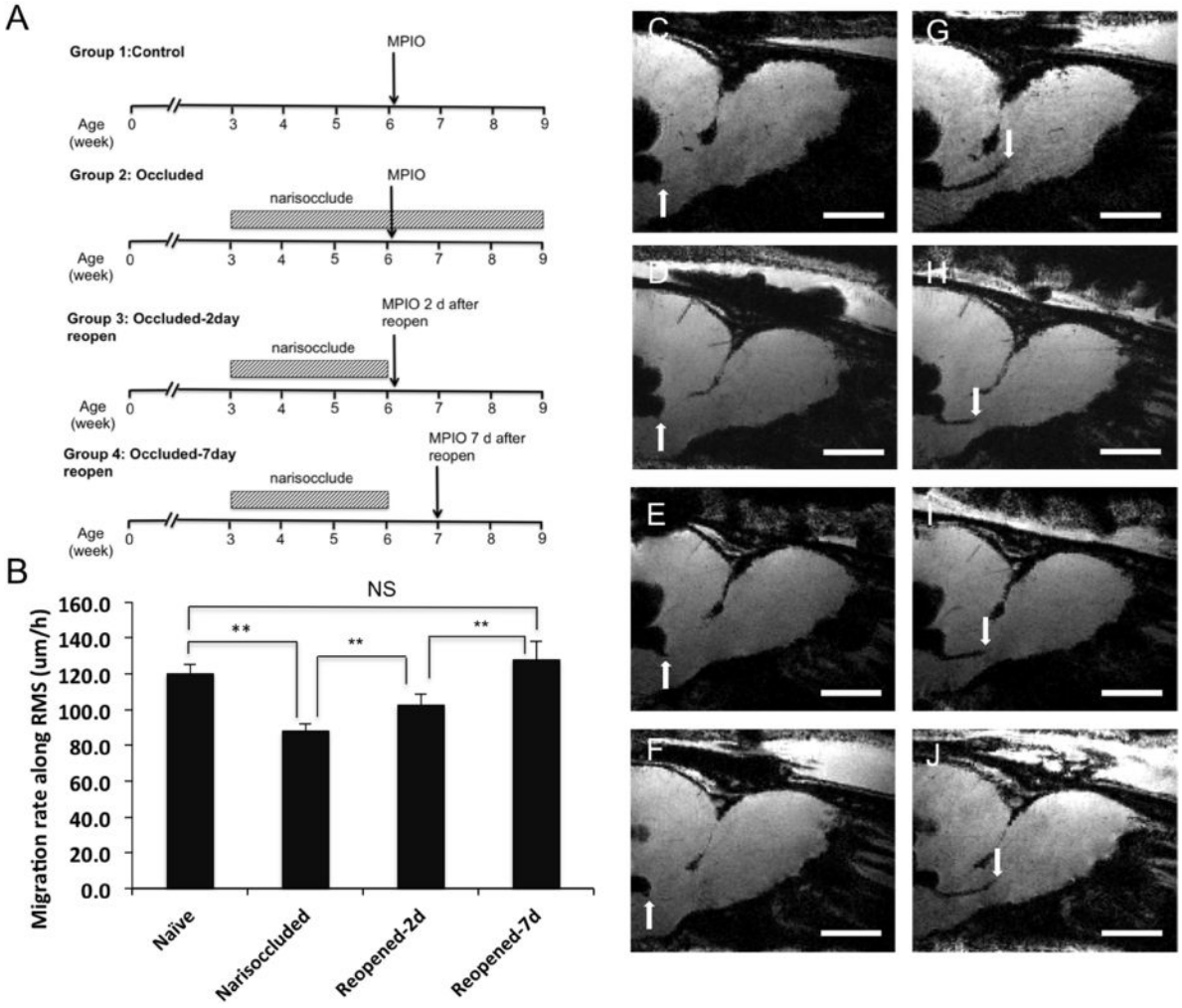

Figure 3.

Effect of olfactory activity on the speed of cell migration from the SVZ along the RMS into the OB. A) Experimental design. B) Migration rate along the RMS. C, D, E, F) MPIOs were injected into lateral ventricles near SVZ and MRI was performed after 4–6 hours after injection to mark the initial time point. Another session of MRI was performed at 22–24 hours post-injection. G, H, I, J) The distance between the first and second time points was measured and divided by the time to calculate the speed of migration graph I. ** Indicates significant difference with p value < 0.05. The numbers of animals in each group were 6 for naïve, 5 for narisoccluded, 5 for 2-day reopened, and 5 for 7-day reopened. Scale bar in images C-J = 2 mm.

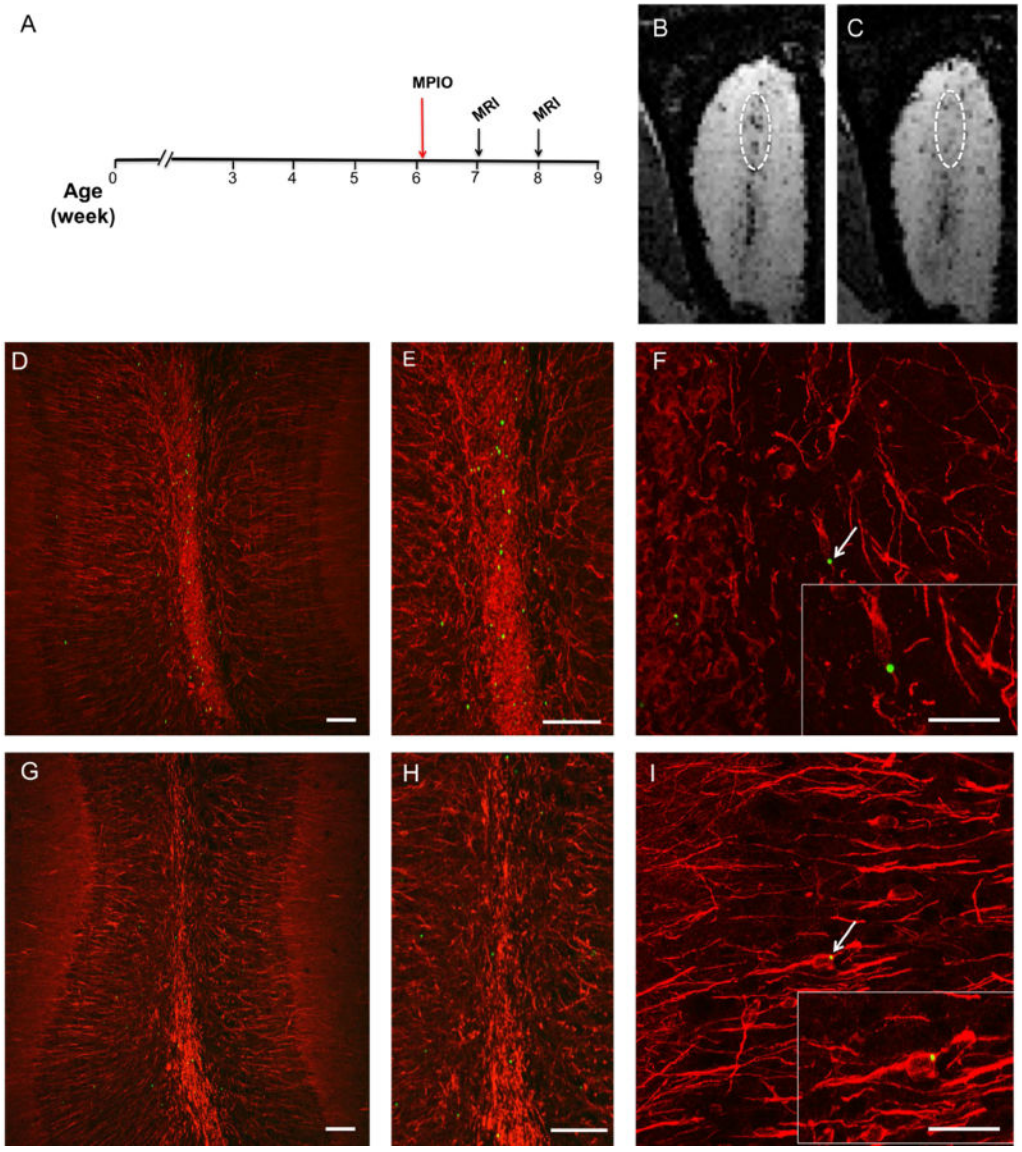

Figure 4.

MRI tracking of radial migration of neuroblast within the OB. time-course of MPIO injection followed by MRI imaging (A). OB images constructed from a minimum intensity projection of the six consecutive MRI slices obtained from 3D images of the OB from a rat that received MPIO injections at 1 week and 2 weeks after MPIO injection, respectively. The images were taken from the same rat. At 1 week, most of MPIO signal accumulated within subependymal layer in the medial plain of the OB (B). At 2 weeks, dark spots spread out into outer layers of the OB indicating the radial migration of cells as they exited from the subependymal zone (C). Histological evaluation of OBs from 1 week (D, E, F) and 2 weeks (G, H, I) post-injected animals revealed similar features and agreed with the MRI results. Immunostaining with doublecortin (red), a marker of immature migrating neurons, showed a co-localization of MPIO (green, marked by arrows and highlighted in the insets of panel F and I) with doublecortin-expressing cells. Scale bar = 40 μm (D, E, G, H) and = 5 μm (F, I)

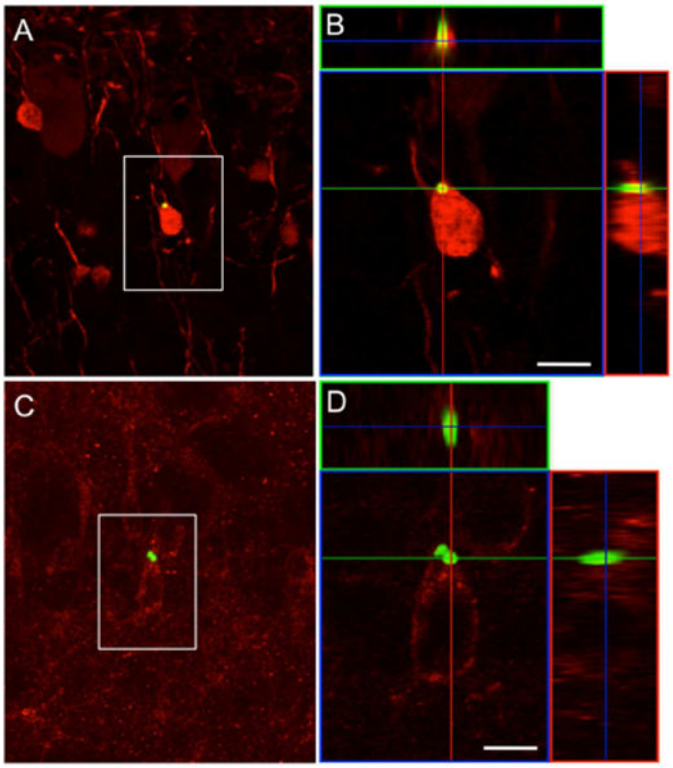

Figure 5.

SVZ neuroblasts that take up the MPIO become interneurons in the OB. (A) Confocal image of a coronal section through the olfactory bulb of a rat that received an MPIO injection in the SVZ 4 weeks prior to tissue processing. The boxed region shows a calretinin-expressing (A) and 5T4-expressing (C) granule cells that contain MPIO particles. (B and D) Confocal 3-D reconstruction of orthogonal projections in the x–z (top) and y–z (right) planes confirms the presence of the MPIO within the cell body. Scale bar = 5 μm.

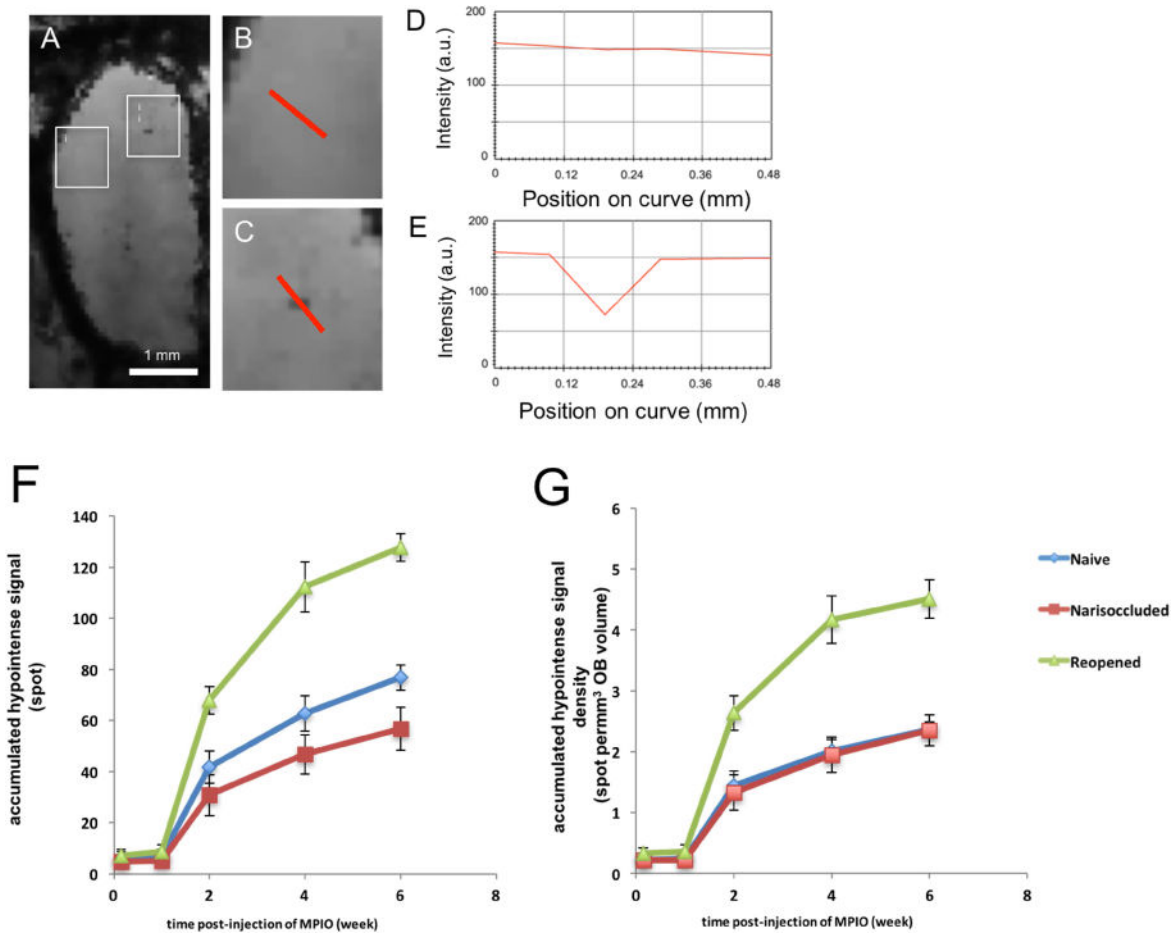

Figure 6.

Assignment of MRI hypointensities as surrogate marker of MPIO(+) cells in the OB and dynamics of new cell addition into the OB. (A) representative image of a single slice (75 μm thick) from 3D MRI image of the OB following 2 weeks after MPIO injection. Appearance of hypointense spots could be seen distributed throughout the OB. (B) Enlarged image of boxes i from (A) that show measurement of signal intensities across the areas that had no hypointense spot (from MPIO). (C) Enlarged image of boxes i from (A) that show measurement of signal intensities across the area with hypointense spot. (D) and (E) show signal intensities across the curves that are shown in red in images B and C, respectively. (F) Graph shows the total numbers of dark pixels found in OB, excluding medial plane that was assigned to subependymal layer. (G) Graph B represents the density of new cells, which derived from graph (F) but taken into the account of OB volume from the corresponding time points.

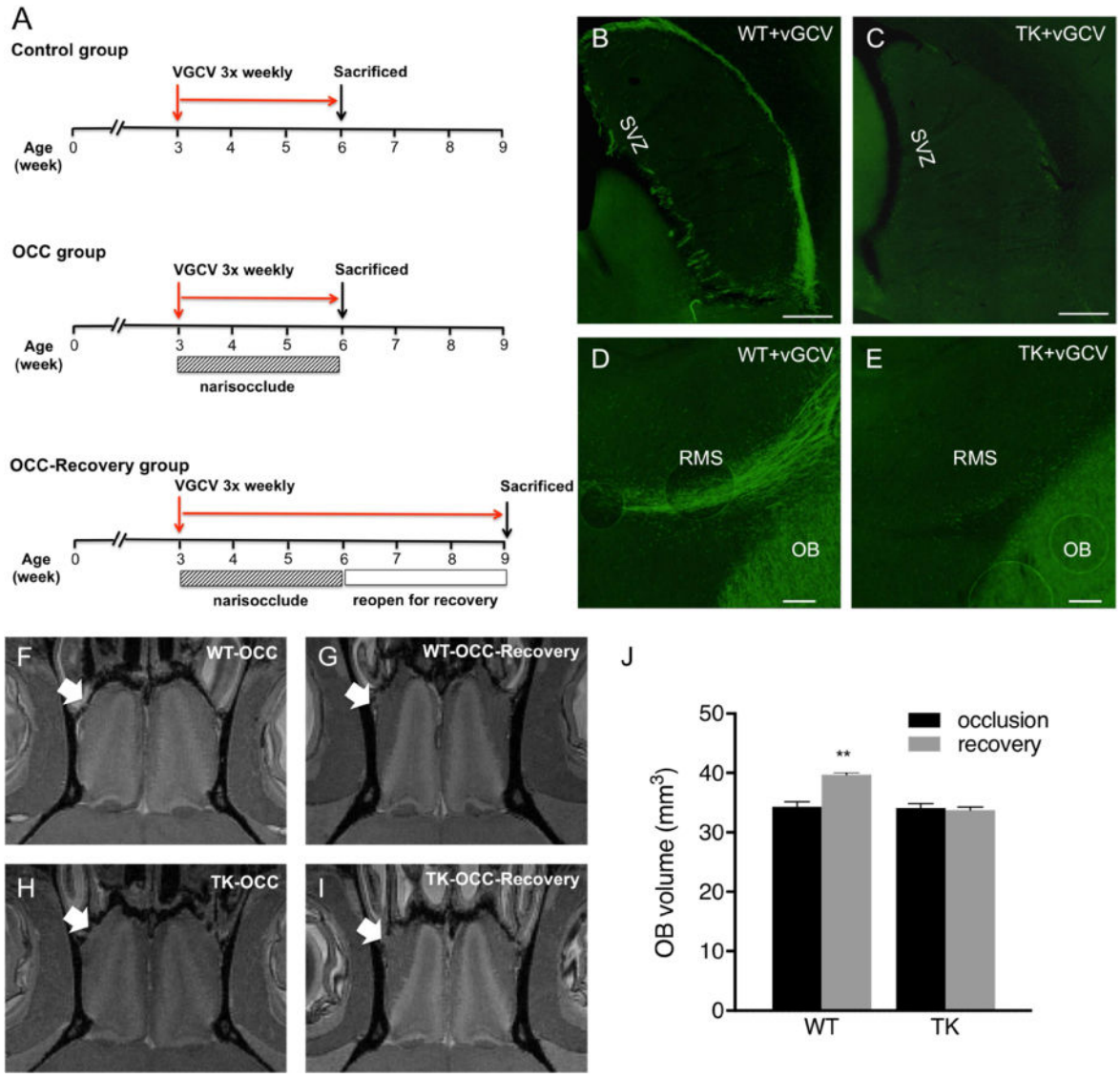

Figure 7.

Pharmacogenetic manipulation of new neuron production. Experimental design (A). Suppression of SVZ neurogenesis via valganciclovir-induced ablation of GFAP-expressing neural precursor cells in GFAP-TK rats (C,E), but not WT rats. (B,C) Doublecortin-immunostaining (green) showed a reduction of DCX (+) migrating neuroblasts from the SVZ and along RMS into the OB. Naris occlusion (OCC) was performed on the WT (WT-OCC) and TK (TK-OCC) rats. Both TK (N=6) and WT (N=4) rats were subjected to naris occlusion for 3 weeks (F,H), and subsequent removal of naris plugs to allow the return of activity for another 3 weeks (G,I). MRI imaging of olfactory bulbs was performed *ex vivo* to obtain OB volumes. Arrows indicate experimental side. As shown in the graph (J), lack of migrating neuroblasts and addition of new neurons led to the loss of OB growth recovery after olfactory activity deprivation. ** Indicates significant difference with $p < 0.05$. Scale bar = 500 μm in A and B, 100 μm in C.